Effect of magnetic field on the photon detection in thin superconducting meander structures

R. Lusche,[1,*] A. Semenov,[1] Y. Korneeva,[2] A. Trifonov,[2] A. Korneev,[2,3,4] G. Gol'tsman,[2,3] and H.-W. Hübers[1,5]

[1]*Institute of Planetary Research, German Aerospace Center (DLR), Rutherfordstrasse 2, 12489 Berlin, Germany*

[2]*Moscow State Pedagogical University, 119991 Moscow, Russia*

[3]*National Research University Higher School of Economics, 20 Myasnitskaya Ulitsa, Moscow 101000, Russia*

[4]*Moscow Institute of Physics and Technology (State University), 9 Institutskiy Pereulok, Dolgoprudny, Moscow Region 141700, Russia*

[5]*Institut für Optik und Atomare Physik, Technische Universität Berlin, Straße des 17. Juni 135, 10623 Berlin, Germany*

(Received 10 September 2013; revised manuscript received 4 February 2014; published 19 March 2014)

We have studied the influence of an externally applied magnetic field on the photon and dark count rates of meander-type niobium nitride superconducting nanowire single-photon detectors. Measurements have been performed at a temperature of 4.2 K, and magnetic fields up to 250 mT have been applied perpendicularly to the meander plane. While photon count rates are field independent at weak applied fields, they show a strong dependence at fields starting from approximately ±25 mT. This behavior, as well as the magnetic field dependence of the dark count rates, is in good agreement with the recent theoretical model of vortex-assisted photon detection and spontaneous vortex crossing in narrow superconducting lines. However, the local reduction of the superconducting free energy due to photon absorption, which is the fitting parameter in the model, increases much slower with the photon energy than the model predicts. Furthermore, changes in the free-energy during photon counts and dark counts depend differently on the current that flows through the meander. This indicates that photon counts and dark counts occur in different parts of the meander.

DOI: 10.1103/PhysRevB.89.104513 PACS number(s): 74.78.Na, 85.25.Oj, 85.25.Pb

I. INTRODUCTION

Vortex motion plays an important role in superconducting meander structures that are used for single-photon detection at visible and near-infrared wavelengths. On the one hand, it can contribute to the generation of dark counts [1,2]. On the other hand, it might explain the detection of near-infrared photons [3–5]. Vortices also reduce critical currents in meander structures. The current transport properties of narrow strips made from thin superconducting films in a magnetic field have been the subject of various studies [6–8]. At sufficiently large fields in a type II superconductor, the current transport is affected by magnetic vortices, which penetrate into the strips. They may even enter the superconductor under the influence of the self field, which is created by a transport current applied to a superconducting meander structure. However, vortices entering the strip are hampered by an energy barrier that is related to the Bean-Livingston surface barrier [9]. This barrier depends on the geometry [10] of the structure, as well as on the applied bias current and magnetic field. Once the barrier is overcome by the vortices, they are dragged across the strip by the Lorentz force and dissipate energy. The dissipated energy might be sufficient to locally destroy superconductivity and generate a dark count event. There are different standpoints if single vortices (and antivortices) cross the strip [1] or vortex-antivortex pairs nucleate within the strip [11,12]. According to Bulaevskii *et al.* [1], thermally activated single-vortex crossings have a significantly lower energy barrier for thin ($d \leq \xi \ll \lambda$) and narrow ($w \ll \Lambda$) strips compared to phase slips and vortex-antivortex depairing. Here, d and w stand for the strip thickness and width, while ξ and Λ are the coherence length and the Pearl length $\Lambda = 2{\lambda_L}^2/d$, and λ_L is the London penetration depth of a magnetic field perpendicular to the film. Bulaevskii *et al.* [1] further state that weak magnetic fields on the order of a few millitesla sufficiently suppress the energy barrier and consequently enhance the rate of vortex crossings over the strip.

Experiments show that the single-photon detection efficiency (DE) of a meander structure is independent on the wavelength up to the cutoff wavelength, which is in the near-infrared spectrum. For photons with less energy, the DE decreases according to a power law [4,13–15]. According to models that describe the photon detection mechanism [3,15], an absorbed photon in a superconductor locally creates a circular cloud of quasiparticles. This "hot spot" then grows and possibly bridges the entire width of the strip. Depending on the photon energy, the superconducting free energy in the hot spot may decrease or vanish, which would destroy superconductivity in a small portion of the strip. The sudden change in resistivity leads to a measurable voltage pulse across the meander structure. Bulaevskii *et al.* [3] calculated the photon count rate (PCR) for the case in which the photon energy is too low to locally convert the superconductor into the normal state. The scenario suggests that vortices cross the strip at the photon absorption site and release the energy $\Phi_0 I$, where Φ_0 is the magnetic flux quantum and I is the current in the strip. This energy, together with the photon energy, is sufficient to destroy superconductivity. The calculations show that dark count rates (DCRs) and vortex-assisted PCRs have different field dependencies and thus can be distinguished. Furthermore, the authors conclude that by application of a field of a few millitesla, the PCR should be enhanced, which would confirm the assistance of vortices in the detection process.

Engel *et al.* [16] investigated DCR and PCR depending on the applied field for a tantalum nitride (TaN) meander up to $|B| = 10$ mT. They have found that the field dependence of the DCR is in accordance with the model predictions of Ref. [3], where crossing vortices are the origin of dark counts.

*Corresponding author: robert.lusche@dlr.de

However, for the magnetic field dependence of the PCR, no evidence was found that vortices assist in the detection process when the photon has insufficient energy to trigger a detection event directly.

Due to the broadband sensitivity, low dark counts, and high detection efficiencies, superconducting meander structures are used in various applications [17]. In order to reach high detection efficiencies, the meanders are biased with almost the highest applicable current. The meander geometry limits this experimental critical current to a value noticeably less than the theoretical depairing current. A meander typically consists of several parallel straight strips, which are a few micrometers long, and bends, which connect the straight parts. Current crowding near the bends increases the local current density and reduces the largest applicable current. In addition, the critical current can be reduced by application of a magnetic field. Theoretically and experimentally, the reduction of the critical current with and without a magnetic field in nonstraight thin-film lines has been studied extensively [3,8,18–21]. The energy barrier of meander structures is lower in the bends than in the straight parts due to the increased current density. This also leads to an increase of the vortex-crossing rate in the bends [18]. Simulations suggest that a meander has spatially dependent sensitivity [22]. According to Ref. [22], absorbed photons in the straight parts are able to trigger a detection event. If photons are absorbed near the inner part of the bend, they cause nucleation of vortices due to the lowered energy barrier but do not trigger a detection event. In contrast, recent modeling states that bends also participate in the detection process [23]. It was found that absorption of a low-energy photon (which creates a relatively small hot spot) in the bend results in a larger voltage pulse than a photon absorbed in the straight part.

In this paper we report on a study of PCRs and DCRs on niobium nitride (NbN) meander structures in magnetic fields up to 250 mT applied perpendicular to the meander plane. We show that a pronounced field dependence of the PCR exists at fields above ±25 mT. We fit our experimental field dependences of PCRs and DCRs with the vortex models of Refs. [1] and [3]. As a fit parameter we use the local reduction of the superconducting free energy at the position of the counting event. We show that the drops of the local free energy associated with photon counts and dark counts behave differently as functions of the applied current and hence support the suggestion that these counts occur in different parts of the meander.

II. MEANDER FABRICATION AND EXPERIMENTAL SETUP

Dark and photon count rate measurements were performed on meanders that were fabricated by deposition of a 4-nm-thick NbN film on an *R*-plane cut sapphire substrate by direct current reactive magnetron sputtering and subsequent patterning by electron beam lithography and ion etching [24]. The meanders with a size of 5.25 × 5 μm^2 are embedded in a 10 × 20 μm^2 matrix of parallel strips with the same strip width and spacing. Embedding a meander in a larger matrix of the same structure eliminates diffraction of light at the meander edges, while the current flows only through the meander structure and hence excludes the surrounding matrix area from photon detection. The meander includes three distinct areas: straight portions (strips), clockwise-oriented bends, and counterclockwise-oriented bends. Two meander types with strip widths of $w = 104$ and 148 nm and spacing between strips of $s = 96$ and 102 nm were investigated. The bends are quadratic areas that connect the parallel strips. The transition temperatures are $T_C = 9.2$ K and 9.3 K, and the critical currents at 4.2 K are 15.2 and 31.8 μA, respectively. An atomic force microscopy (AFM) image of an NbN meander is displayed in the inset of Fig. 1. The second inset shows the current-voltage (I-V) curve of an NbN meander at 4.2 K.

For the experiments we used a homemade ^{4}He variable temperature insert (VTI) in the form of a dipstick cryostat with attached superconducting solenoid. This setup was immersed in a standard 100-L ^{4}He transport dewar and operated at a temperature of 4.2 K. Magnetic fields up to 2 T were applied perpendicular to the meander plane. The meanders were fixed to a sample holder made of copper that contains a temperature sensor, heater, calibrated micro-Hall sensor, optical fiber, and coaxial cable to guide the electrical signals. For studying DCRs the end of the fiber that is outside the VTI was light-tight covered. For illumination measurements a halogen lamp was used, with a subsequent prism monochromator for wavelength selection from 300 to 3000 nm. The unpolarized light was coupled into a standard multimode fiber (core diameter, 200 μm; numerical aperture, 0.39) by a collimator lens and guided to the meander. The fiber has a transmission window from 400 to 2200 nm and hence covered the important part of the spectrum.

The meanders were illuminated from the rear side, i.e., through the sapphire substrate. Therefore, the photon flux incident upon the structure could not be precisely determined. The meanders were directly connected to the coaxial cable,

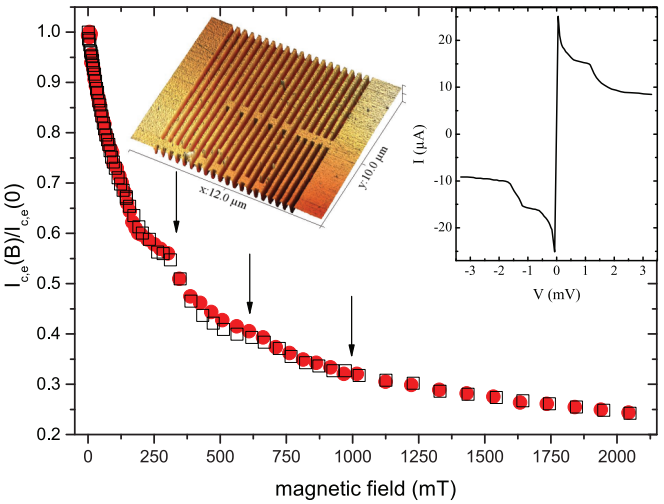

FIG. 1. (Color online) Dependence of the normalized critical current on the applied magnetic field of the NbN meander with 148-nm-wide strips. The solid circles are measured values of $I_{c,e}(B)/I_{c,e}(0)$ for positive field values, whereas the squares are for negative fields. For clarity, the latter are mirrored at the y axis. The inset shows an AFM picture of an NbN meander and an I-V curve at 4.2 K.

which led voltage pulses out of the VTI to a 48-dB amplifier and a 200-MHz pulse counter and was simultaneously used to supply the bias current. Biasing was done by a homemade low-noise tunable voltage source via a bias tee, which was inserted after the coaxial feed through at the VTI.

Wavelengths used for illumination are at least a three times larger than the wire width but remain less than the size of the meander area and the embedding matrix. The overall absorbance of the meander depends on the light polarization. The absorbance is larger for light, which is polarized parallel to the meander lines [25]. This, however, does not affect the distribution of the absorption probability for a photon on the meander. The photon detection mechanism also is not affected by the polarization, because a photon is absorbed locally by only one electron. Although the presence of the bends in the meander complicates the interpretation of the photon detection, using the meander structure tremendously increases optical coupling. In contrast to a meander, working with a single strip would require very large light intensities in order to achieve measurable PCRs. Intense illumination would also increase the probability of multiphoton events and decrease the critical current via heating.

III. RESULTS AND DISCUSSION

A. Critical current

In order to evaluate the symmetry of the applied field, possible offsets, and hysteresis effects, we performed measurements of the experimental critical current $I_{c,e}$ depending on the applied magnetic field. The magnetic field was set to a certain value, and the current was slowly increased until the superconducting state was destroyed. This procedure was repeated at least three times to improve the accuracy of the $I_{c,e}$ values. The uncertainty of the measurement is determined by the statistical variations, along with the 0.1-μA accuracy of the bias current source.

Figure 1 exemplarily displays the dependence of the critical current $I_{c,e}(B)$ on the applied magnetic field for the meander with a 148-nm strip width. The data are normalized to the zero field value $I_{c,e}(0)$. The measurements in negative applied field (squares) are mirrored on the y axis in order to visualize potential asymmetries. Both curves are symmetric except for a small range at intermediate fields between 300 and 500 mT. Coming from weak fields, the normalized $I_{c,e}(B)$ shows a linear dependence in the Meißner phase up to $\sim$125 mT. With increasing field strength, vortices enter the strip, hence the critical current transitions into the Shubnikov mixed phase that is characterized by a much flatter slope. Here, a pronounced step is visible at $\sim$285 mT, followed by a step at 620 mT (indicated by the arrows in Fig. 1). A small third step at 940 mT (negative magnetic field, squares) can also be observed. The steps are fairly equidistant, with a separation of $\Delta B \approx 330$ mT. The meander with a 104-nm strip width exhibits similar pronounced steps at fields of $\sim$265, 577, and 883 mT. These steps have been observed before in superconducting thin films [26–29]. Karapetrov *et al*. [27] ascribe the appearing kinks to structural reordering of the vortices due to the magnetic field within the film. It was found that the appearance of kinks with the magnetic field is quadratic. A reason for the deviation to our results might be the different $\kappa = \lambda/\xi$ values. We use a thin NbN film with a value of $\kappa = 55.2$, whereas in Ref. [27] thick Nb samples with $\kappa = 6.6$ were used. Furthermore, our NbN samples show quite strong pinning. Closer accordance is found in recent simulations by Vodolazov [30]. Vodolazov states that each time the magnetic field is sufficiently large, a new row is nucleated in the strip, leading to an additional step. Figure 2(b) of Ref. [30] displays the calculated current dependence on the field with visible equidistant steps. In order to compare our measurement with the calculations, the field axis has to be normalized to $B_{C2} = \Phi_0/2\pi\xi^2(T) = 9.36$ T, with the coherence length $\xi(4.2\ \mathrm{K}) = 5.93$ nm and the diffusivity $D = 0.51\ \mathrm{cm}^2/\mathrm{s}$. Qualitatively, the result is in accordance with the calculations in Ref. [30] carried out for straight lines. Small quantitative differences are not surprising, since in a meander the critical current is largely defined by the bends.

The dependence of the critical current on the field in the Meißner phase was studied theoretically (e.g., in Refs. [3] and [6]). For our types of meanders, in terms of the strip width and thickness, a linear dependence of the field is predicted:

$$\frac{I_C(B)}{I_C(0)} = 1 - \frac{B}{B_{S,t}}R, \tag{1}$$

where $I_C(B)$, $I_C(0)$ are the critical currents in a straight strip in the presence or absence of a magnetic field and R is a correction factor. According to Maksimova [6], $B_{S,t} = 2\lambda^2\mu_0 I_C(0)/w^2 d$ (μ_0 is the vacuum permeability) is the calculated field for entry of the first vortex in a straight strip. Ideally, the critical current in a meander is the critical current in the bends. In real meanders, local impurities and geometric imperfections of the meander line can further reduce the experimental critical current. Hence, in order to be applicable for meanders, a correction factor R is introduced in Eq. (1) to account for all geometry-related effects. Following Clem *et al*. [8], a critical current reduction of $\sim$50% is expected due to rectangular 180° bends, leading to values of R around 0.5. However, various simplifications were assumed in these calculations; e.g., the vortex core energy was neglected, leading to only qualitative results. From the theory described in Ref. [3], the following values are expected: $B_{S,t} = \Phi_0/e\pi\xi w = 393$ mT ($w = 104$ nm) and $B_{S,t} = \Phi_0/e\pi\xi w = 276$ mT ($w = 148$ nm), where e is Euler's number. We used R as the only fitting parameter and obtained $R = 0.7$ ($w = 104$ nm) and $R = 0.83$ ($w = 148$ nm). These R values are consistent with reduction factors calculated as $R = I_{c,e}/I_{c,s}$, where $I_{c,e}$ is the experimental critical current at zero magnetic field and $I_{c,s} = 2w\Phi_0 d/2e\pi\xi\lambda^2$ is the critical current calculated for a straight line according to Bulaevskii *et al*. [3]. Our values also agree with the reduction factor obtained by Engel *et al*. [16] for the same meander geometry. In the following we use the experimentally found $B_S = B_{S,t}/R$ for our calculations.

B. Photon counts

PCRs were obtained as an average from three successive runs. In each run, counts were recorded within 1 s. Magnetic fields were applied in steps from 3 mT at weak fields up to 10 mT close to the upper critical field. Dark counts were always subtracted, although they typically amounted to less than 1% of the recorded counts.

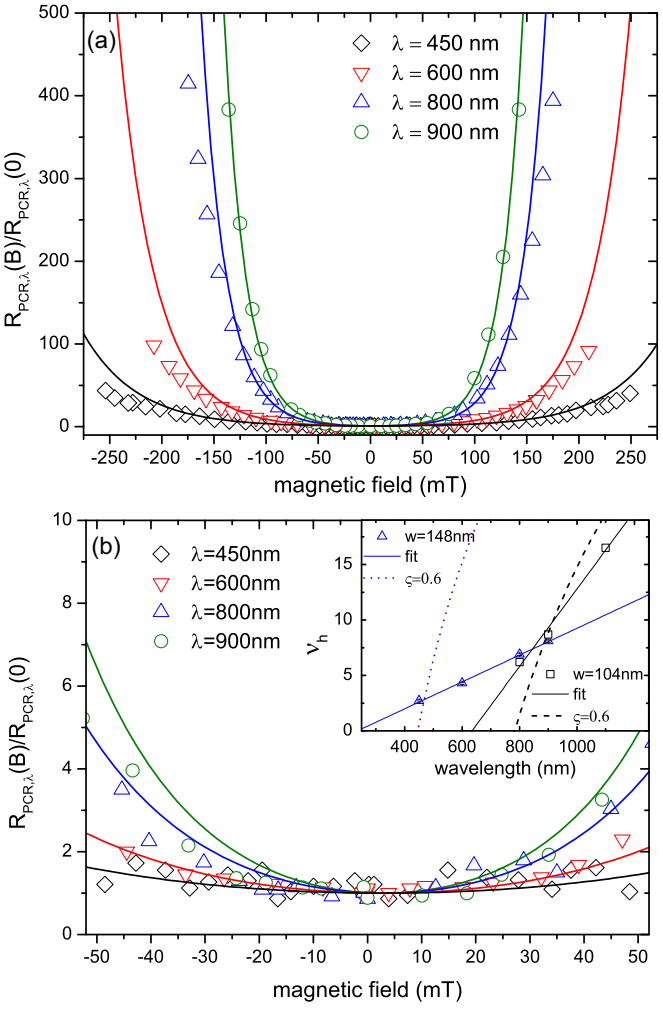

FIG. 2. (Color online) (a) Normalized PCRs vs magnetic field for the NbN meander with a strip width of $w = 148$ nm at a fixed bias current of $0.57I_{c,e}$ for four illumination wavelengths. The solid lines represent fits with Eq. (2). (b) Detailed view of (a) for weak fields between ±50 mT. In the inset, ν_h values vs illumination wavelength are shown. The symbols are the values obtained from fits with Eq. (2). The solid lines are fits to the experimental data, and the dashed and dotted lines are theoretical curves of ν_h, which are calculated according to Eq. (3).

Figure 2(a) shows the normalized dependence of the PCR on the applied magnetic field for the meander with $w = 148$ nm. PCRs were measured for four wavelengths. A bias current of 18.2 μA was chosen because it was the best compromise between having enough photon counts, for which higher currents are favorable, and strong field dependence, which increases at low currents. The meander with a 104-nm strip width was current biased with 11 μA. As shown by Engel *et al.* [16], the PCR does not depend on the field for values up to ±10 mT. With our accuracy we do not see any changes up to ±25 mT (Fig. 2(b)). However, at larger fields the count rate starts to increase. Illumination of the meander with low-energy photons (900 nm) results in a stronger field dependence that raises the PCR by three or four orders of magnitude compared to higher energy photons (450 nm), where the PCR increases by only one or two orders. This is consistent with the argument [4] that photons with wavelengths that are considerably larger than the cutoff wavelength need more "assistance" by vortices to be counted than those with wavelengths closer to the cutoff.

Before comparing our data with the model of Ref. [3], note that model calculations were carried out for straight lines, whereas photon counts in a meander can originate from the straight parts or from the bends. Furthermore, the current direction in the bends (clockwise or counterclockwise) viewed along the field direction is crucial. In counterclockwise bends the current density will be increased by the external field due to screening currents, while in clockwise bends it will be decreased. For photon detection and dark counts in an external magnetic field, an ideal meander presents three distinct areas, among which counterclockwise bends will have the lowest energy barrier and hence the largest probability for vortex entry. Although photon absorption sites are uniformly distributed over the meander, vortex-assisted photon counts originate from sites where the barrier is strongly reduced. For large photon energies, photon counts come predominantly from straight lines since they occupy a much larger area of the meander structure as the bends. The field created in a meander line by the current in all other lines is on the order of a few tens of microtesla [16]. Therefore, the lines at the meander edges will have the same vortex barrier as the lines in the middle of the meander.

We now fit our data with the model of Ref. [3], where in Eq. (45) the vortex-assisted PCR in the absence of a magnetic field is defined as $R_{\rm PCR} = R_h(1 - \exp(-2\eta))$. Here, R_h denotes the rate of formation of hot spots, which have enough energy to trigger a detection event. Following the arguments in Ref. [16], i.e., that for bias currents close to the experimental critical current and for high-energy photons the condition $DE \approx R_h$ is reached, we conclude that for the bias current $0.57I_{c,e}$, the count rate related to its maximum value is well below 1: $R_{\rm PCR}(0.57I_{c,e})/R_h = 1 - \exp(-2\eta) \leq 10^{-3} \approx 2\eta$. For $\eta \ll 1$ and a small bias current, the normalized vortex-assisted PCR with an applied magnetic field (Ref. [3], Eq. (47)) can be simplified to

$$\frac{R_{\mathrm{PCR},\lambda}(B)}{R_{\mathrm{PCR},\lambda}(0)} \approx \cosh\left(\frac{(\nu_h + 1)}{B_S}\frac{I_{c,e}}{I_b}B\right). \qquad (2)$$

Here, $I_{c,e}$ is the experimental critical current, which we identify as the current for which the energy barrier vanishes in straight lines. The parameter ν_h accounts for the suppression of the superconducting condensation energy in the hot spot due to photon absorption. It represents the dimensionless energy of a vortex inside the hot spot. We fitted Eq. (2) to the data up to magnetic fields of ∼125 mT, where we are certain that the field has no effect on the bias current. Above ∼125 mT the measured normalized PCRs in negative, as well as positive, fields show deviations from the expected field dependence. This is especially pronounced for the three largest rates at 450 nm. The reason for this deviation is the influence of the field on the bias current. With increasing field, the critical current decreases until it is equal to the bias current. Close to this point the field might increase the average resistance of the meander. Since we are using a constant voltage source, the bias current decreases, leading to considerably lower count rates.

The results of fitting are displayed in Fig. 2(a) by the solid lines. Since the photon energy is not explicitly included in

the model of Ref. [3], ν_h was used as the fitting parameter. The inset of Fig. 2(b) shows the dependence of ν_h on the illumination wavelength for both meanders. The size of each symbol corresponds to the measurement uncertainty. This dependence is linear for both studied meanders, with slopes of $1.21\nu_h/100$ nm (meander with $w = 148$ nm) and $3.5\nu_h/100$ nm (meander with $w = 104$ nm). In order to compare the ν_h values, we adopt the assumption of Ref. [3] that the cloud of quasiparticles has uniform density and spans the entire width w of the strip with the thickness d. The effective photon energy thus homogenously reduces the superconducting condensation energy F in the volume w^2d. With the relation $F = \varepsilon_0(w/\xi)^2/(4\pi)$, where ε_0 is the characteristic vortex energy in a thin film (Ref. [3], Eq. (8)), we find the reduced value of the dimensionless vortex energy in the hot spot:

$$\nu_h = \nu_0 - 4\pi\varsigma\frac{hc}{\lambda}\frac{1}{k_BT}\frac{\xi^2}{w^2}. \tag{3}$$

The coefficient $0 < \varsigma < 1$ accounts for losses of the photon energy via electron-phonon interaction and via phonon escape into the substrate. The above dependence of ν_h is also plotted in the inset of Fig. 2(b) for both meanders, with $\nu_0 = 82$ and $\varsigma = 0.6$ (dotted line) for $w = 148$ nm and $\nu_0 = 96$ and $\varsigma = 0.6$ (dashed line) for $w = 104$ nm. The slopes of the theoretical wavelength dependence of ν_h are significantly steeper than the experimental data show. The reason for this deviation might be the assumption of a uniform density of quasiparticles in the hot spot, which does not hold for our meanders [31].

Illumination of the meander with light of a fixed wavelength while varying the bias current should reveal the relation between the photon energy hc/λ and ν_h. Therefore, we measured PCRs for currents from $0.56I_{c,e}$ to $0.87I_{c,e}$ at the wavelength of 900 nm. Figure 3 depicts the normalized PCRs for fields below ± 125 mT. The field dependence of PCRs weakens with increasing bias current. This is consistent with a shift of the cutoff toward longer wavelengths [4] and shows

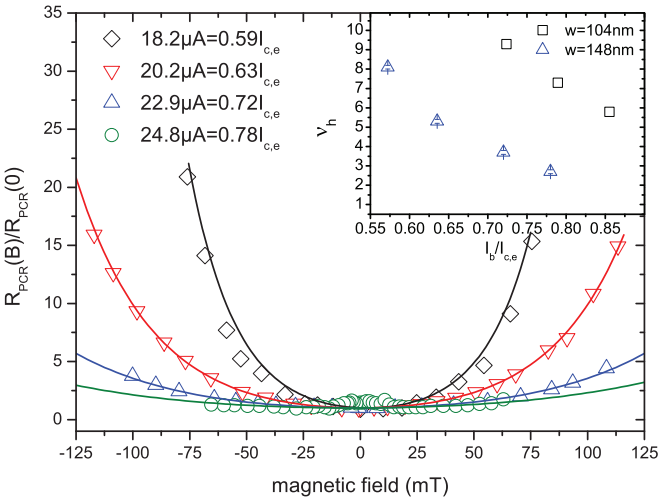

FIG. 3. (Color online) PCRs $R_{\rm PCR}(B)$ normalized to the zero field value $R_{\rm PCR}(0)$ vs the applied magnetic field at a fixed illumination wavelength of 900 nm. The PCRs at four bias currents of the meander with $w = 148$ nm are plotted. The inset shows the ν_h values obtained by the fit of Eq. (2) to the experimental data of both meanders.

that vortices become less important to assist photon counts as the current increases.

The simplification that leads to Eq. (2) might not be appropriate for currents close to $I_{c,e}$. Therefore, in order to fit the field dependences at large currents, we used the field-dependent terms for the vortex and antivortex crossing (according to Ref. [3], Eq. (28)):

$$\frac{R_{\rm PCR}(I,B)}{R_{\rm PCR}(I,0)} = \left(1 + \frac{I_{c,e}}{B_S I_b}B\right)^{(\nu_h+1)} + \left(1 - \frac{I_{c,e}}{B_S I_b}B\right)^{(\nu_h+1)}. \tag{4}$$

Although the theoretical field dependence of the photon counts due to vortex crossings fits well to our experimental data over a range of applied bias currents, the fit parameter ν_h decreases noticeably with the applied bias current. This is shown in the inset in Fig. 3. In the framework of the model, variations of ν_h with the current can be understood as if the photon counts at larger currents would originate from the parts of the meander where the photon with the same energy reduces the barriers for vortex entries by a lesser amount.

C. Dark counts

Dark counts could not be analyzed in the same range of bias currents as PCRs since they are practically nonobservable at bias currents from $0.47I_{c,e}$ to $0.63I_{c,e}$. Even at larger currents the rates are very low. Therefore, dark counts were accumulated several times within a 10-s window, and the average rate was then computed. Figure 4(a) displays normalized DCRs for four ($w = 148$ nm) and three ($w = 104$ nm) bias currents. With increasing current, the field dependence for both meanders becomes slightly weaker. According to Ref. [3], dark counts originate from vortex and antivortex crossings, and the field-dependent rate reads

$$\frac{R_{\rm DCR}(I,B)}{R_{\rm DCR}(I,0)} = \left(1 + \frac{I_{c,e}}{B_S I_b}B\right)^{(\nu_0+1)} + \left(1 - \frac{I_{c,e}}{B_S I_b}B\right)^{(\nu_0+1)}. \tag{5}$$

Fitting delivered ν_0 values with a quite large uncertainty because of the spread of experimental data points. However, both meanders exhibit the same, current-independent ν_0 values as displayed in Fig. 4(b). This current-independent behavior of ν_0 is expected from the theory [3] in which

$$\nu_0 = \frac{\Phi_0^2\mu^2 d}{8\pi\lambda^2\mu_0 k_B T}. \tag{6}$$

Here, μ^2 describes the order parameter suppression due to the bias current. This is the only parameter that depends on the current. However, μ^2 can safely be taken equal to unity for the applied currents, since they are sufficiently smaller than the theoretical depairing current.

The different current dependences of the dimensionless vortex energy ν_h for the PCR and ν_0 for the DCR can be understood if one suggests that counts occur in different parts of the meander. If vortex-assisted photon count events were triggered by vortices in the same area of the meander as the dark counts, a similar dependence of ν_h and ν_0 on the bias current would be expected. Without illumination, vortex

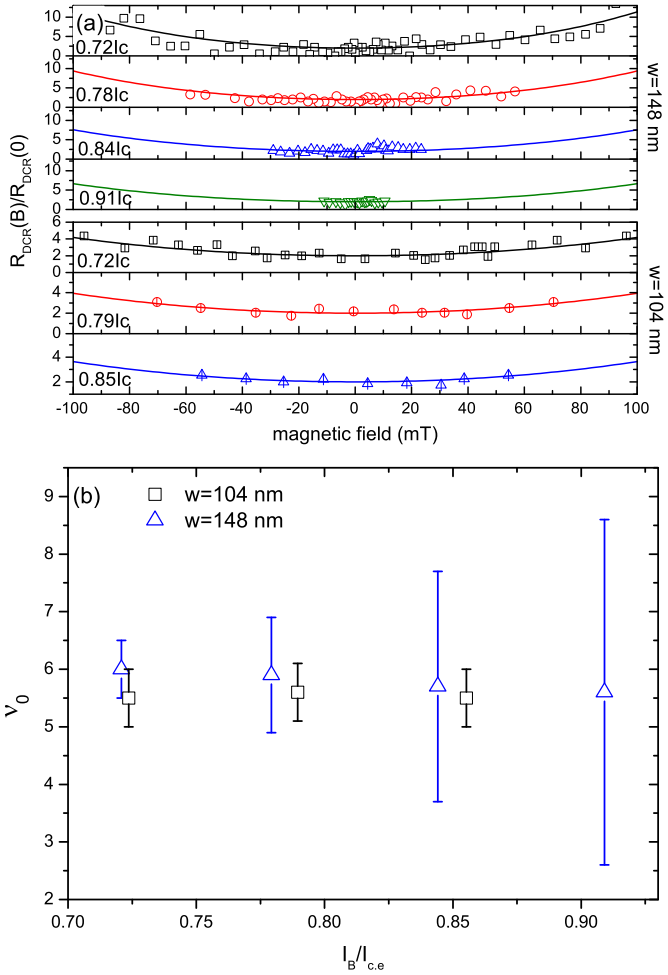

FIG. 4. (Color online) (a) Normalized DCRs vs magnetic field for four ($w = 148$ nm) and three ($w = 104$ nm) bias currents. The solid lines represent fits with Eq. (5). (b) ν_0 values as a function of the relative bias current obtained by the fit with Eq. (5).

crossings are more probable in the bends of the meander due to the elevated current density and lower energy barrier. Although the bias current reduces the barrier, it always remains smaller in the bends. Consequently, dark counts originating from vortex crossings are more likely to occur in the bends. The same applies to photon counts for small photon energies when the reduction of the free energy around the absorption site is relatively low. A photon with larger energy, when it is absorbed in the straight portion of the meander line, reduces locally the energy barrier to a value comparable to the barrier in the bends. At this point the straight lines begin to contribute to PCRs. At even larger energies photons absorbed in the lines dominate the PCRs since the meander area associated with straight lines is more than an order of magnitude larger than the area associated with the bends. This explanation is consistent with the earlier observed difference [32] in electrical amplitudes of the dark counts and photon counts for photons with large energies, as well as with the similarity of amplitudes of the dark counts and photon counts at low photon energies.

IV. CONCLUSION

We have studied the influence of a magnetic field on PCRs and DCRs in ultrathin NbN meander structures for different photon wavelengths and bias currents. We have shown that the field dependences of both count rates are described well by the model that proposes vortex crossing of the meander line as the mechanism of the dark counts and the assisting mechanism for photon counts. By fitting this model to the experimental data, we have found that the vortex energy at the site from which the count originates depends differently on the bias current for photon and dark counts. The vortex energy is almost current independent for dark counts and decreases with the current for photon counts. We have explained this observation, suggesting that dark counts originate predominantly from bends while the photon counts may occur in different parts of the meander depending on the photon energy and the current. Increasing the photon energy and the current increases the contribution of photon counts, which originate from the straight lines in the meander.

ACKNOWLEDGMENTS

We thank D. Vodolazov for helpful discussions. R.L. acknowledges support by the Helmholtz Research School on Security Technologies. Y.K., A.T., A.K., and G.G. acknowledge support by Russian Foundation for Basic Research Grant No. 12-02-31841 and Russian state Contract 14.B25.31.0007 from the Ministry of Education and Science of the Russian Federation.

[1] L. N. Bulaevskii, M. J. Graf, C. D. Batista, and V. G. Kogan, Phys. Rev. B **83**, 144526 (2011).
[2] H. Bartolf, A. Engel, A. Schilling, K. Ilin, M. Siegel, H. W. Hübers, and A. Semenov, Phys. Rev. B **81**, 024502 (2010).
[3] L. N. Bulaevskii, M. J. Graf, and V. G. Kogan, Phys. Rev. B **85**, 014505 (2012).
[4] M. Hofherr, D. Rall, K. Ilin, M. Siegel, A. Semenov, H.-W. Hübers, and N. A. Gippius, J. Appl. Phys. **108**, 014507 (2010).
[5] A. N. Zotova and D. Y. Vodolazov, Phys. Rev. B **85**, 024509 (2012).
[6] G. Maksimova, Phys. Solid State **40**, 1607 (1998).
[7] B. L. T. Plourde, D. J. Van Harlingen, D. Y. Vodolazov, R. Besseling, M. B. S. Hesselberth, and P. H. Kes, Phys. Rev. B **64**, 014503 (2001).
[8] J. R. Clem, Y. Mawatari, G. R. Berdiyorov, and F. M. Peeters, Phys. Rev. B **85**, 144511 (2012).
[9] C. Bean and J. Livingston, Phys. Rev. Lett. **12**, 14 (1964).
[10] G. Stan, S. B. Field, and J. M. Martinis, Phys. Rev. Lett. **92**, 097003 (2004).
[11] T. Yamashita, S. Miki, K. Makise, W. Qiu, H. Terai, M. Fujiwara, M. Sasaki, and Z. Wang, Appl. Phys. Lett. **99**, 161105 (2011).

[12] G. R. Berdiyorov, M. V. Milosevic, and F. M. Peeters, Phys. Rev. B **79**, 184506 (2009).
[13] A. Engel, A. Aeschbacher, K. Inderbitzin, A. Schilling, K. S. Ilin, M. Hofherr, M. Siegel, A. D. Semenov, and H.-W. Hubers, Appl. Phys. Lett. **100**, 062601 (2012).
[14] A. Verevkin, J. Zhang, R. Sobolewski, A. Lipatov, O. Okunev, G. Chulkova, A. Korneev, K. Smirnov, G. N. Goltsman, and A. Semenov, Appl. Phys. Lett. **80**, 4687 (2002).
[15] A. Semenov, A. Engel, H.-W. Hübers, K. Ilin, and M. Siegel, Eur. Phys. J. B **47**, 495 (2005).
[16] A. Engel, A. Schilling, K. Ilin, and M. Siegel, Phys. Rev. B **86**, 140506 (2012).
[17] C. M. Natarajan, M. G. Tanner, and R. H. Hadfield, Supercond. Sci. Tech. **25**, 063001 (2012).
[18] J. R. Clem and K. K. Berggren, Phys. Rev. B **84**, 174510 (2011).
[19] H. L. Hortensius, E. F. C. Driessen, T. M. Klapwijk, K. K. Berggren, and J. R. Clem, Appl. Phys. Lett. **100**, 182602 (2012).
[20] D. Henrich, P. Reichensperger, M. Hofherr, J. Meckbach, K. S. Il'in, M. Siegel, A. D. Semenov, A. Zotova, and D. Y. Vodolazov, Phys. Rev. B **86**, 144504 (2012).
[21] O.-A. Adami, D. Cerbu, D. Cabosart, M. Motta, J. Cuppens, W. A. Ortiz, V. V. Moshchalkov, B. Hackens, R. Delamare, J. Van de Vondel, and A. V. Silhanek, Appl. Phys. Lett. **102**, 052603 (2013).
[22] G. R. Berdiyorov, M. V. Milosević, and F. M. Peeters, Appl. Phys. Lett. **100**, 262603 (2012).
[23] A. Zotova and D. Vodolazov, Supercond. Sci. Technol. **26**, 075008 (2013).
[24] G. N. Goltsman, K. Smirnov, P. Kouminov, B. Voronov, N. Kaurova, V. Drakinsky, J. Zhang, A. Verevkin, and R. Sobolewski, IEEE Trans. Appl. Supercond. **13**, 192 (2003).
[25] A. D. Semenov, B. Günther, U. Böttger, H.-W. Hübers, H. Bartolf, A. Engel, A. Schilling, K. Ilin, M. Siegel, R. Schneider, D. Gerthsen, and N. A. Gippius, Phys. Rev. B **80**, 054510 (2009).
[26] T. Yamashita and L. Rinderer, J. Low Temp. Phys. **24**, 695 (1976).
[27] G. Karapetrov, V. Yefremenko, G. Mihajlović, J. E. Pearson, M. Iavarone, V. Novosad, and S. D. Bader, Phys. Rev. B **86**, 054524 (2012).
[28] S. H. Brongersma, E. Verweij, N. J. Koeman, D. G. de Groot, R. Griessen, and B. I. Ivlev, Phys. Rev. Lett. **71**, 2319 (1993).
[29] J. Guimpel, L. Civale, F. de la Cruz, J. M. Murduck, and I. K. Schuller, Phys. Rev. B **38**, 2342 (1988).
[30] D. Y. Vodolazov, Phys. Rev. B **88**, 014525 (2013).
[31] A. Engel and A. Schilling, J. Appl. Phys. **114**, 214501 (2013).
[32] P. Haas, A. Semenov, H.-W. Hübers, J. Beyer, A. Kirste, T. Schurig, K. Il'in, M. Siegel, A. Engel, and A. Smirnov, IEEE Trans. Appl. Supercond. **17**, 298 (2007).